Earth, Planets and Space

EXPRESS LETTER

Open Access

An evaluation of space weather conditions for FORMOSAT-3 satellite anomalies

Han-Wen Shen[1], Jih-Hong Shue[1*], John Dombeck[2] and Tsung-Ping Lee[3]

Abstract

The variable electromagnetic environment in geospace plays a crucial role in influencing the occurrence probability of satellite anomalies. FORMOSAT-3 (FS3) is a Low-Earth-Orbit (LEO) mission, which consists of six identical microsatellites that orbit in the altitude of 700–800 km and with an inclination of 72°. The dependences of the FS3 satellite anomalies on space weather conditions have not been investigated in the past. With an exception of a small number of extremely high geomagnetic events, we find that the occurrence rate of the FS3 anomalies is negatively correlated with the level of geomagnetic activity. Moreover, the relationship between numbers of anomalies and sunspots is also anti-correlated. A superposed epoch analysis demonstrates that the intensity of galactic cosmic rays (GCR) is relatively high at the times of the anomalies. All these results infer that the FS3 anomalies predominantly occurred under the conditions associated with low solar activity. The possible main cause for the FS3 anomalies is high-energy trapped protons or GCR. In summary, this paper presents a statistical result that a satellite can be prone to suffer an anomaly under low solar or geomagnetic activity.

Keywords: Satellite anomaly, FORMOSAT-3, Low earth orbit, Space weather, Geomagnetic activity, Solar cycle, Galactic cosmic rays

Introduction

The instruments mounted on satellites contain a substantial amount of highly sensitive electronics. Many previous studies have suggested that charged particles can seriously influence the operation of satellite electronics in the space environment. Love et al. (2000) reported that several failures of the Geostationary-Earth-Orbit (GEO) satellites were associated with a highly variable electron environment. Baker (2000) pointed out that the failures of MARECS-A in February 1986, Telstar 401 in January 1997, and Galaxy 4 in May 1998 were caused by charged particles and subsequent electrostatic discharges. Gubby and Evans (2002) suggested that protons with energies over 1 MeV or electrons with energies over 0.5 MeV can effectively lead to malfunctions on satellite electronics. Pilipenko et al. (2006) proposed that high flux of solar energetic protons (>1 MeV) is the main risk factor that causes anomalies during solar maximum and that relativistic electrons are responsible for the anomalies that occurred during the periods between solar minimum and solar maximum. Iucci et al. (2005) investigated the satellite anomalies in different orbits during the period of 1986–1994. They found that the anomalies recorded by the satellites in high-altitude near-polar orbits were related to high-energy protons, and the anomalies recorded by the satellites in GEO and low-altitude near-polar orbits were related to high-energy electrons. All these studies inferred that satellite anomalies are frequently related to charged particles.

The variations in the flux, energy, and spatial distribution of charged particles play an imperative role in controlling the occurrence probability of satellite anomalies. High solar activity produces Coronal Mass Ejections (CMEs) and other special solar wind structures to influence Earth's magnetosphere (Liu et al. 2011; Möstl et al. 2010). The high-speed solar wind, energetic charged

*Correspondence: jhshue@jupiter.ss.ncu.edu.tw
[1] Department of Space Science and Engineering, National Central University, Taoyuan, Taiwan
Full list of author information is available at the end of the article

particles, and large southward interplanetary magnetic fields (IMF) associated with these structures can have drastic impacts on the electromagnetic environment of Earth, resulting in more solar wind energy going into the magnetosphere and enhancing the level of geomagnetic activity (Gonzalez et al. 1994; Kamide 1992). During periods of high geomagnetic activity, plasma properties would vary and then cause several kinds of influences on satellites, such as single event effects, satellite charging, and total dose effects (Guenzer et al. 1979; Kolasinski et al. 1979; Anderson et al. 1994; Bashkirov et al. 1999; Ferguson et al. 2011; Loto'aniu et al. 2015). Indeed, most previous studies have suggested that many satellite anomalies were attributed to high geomagnetic activity (e.g., Belov et al. 2004; Choi et al. 2011; Farthing et al. 1982; Fennell et al. 2001; Iucci et al. 2005; Lohmeyer et al. 2015; Loto'aniu et al. 2015; Nichitiu et al. 2004; O'Brien 2009; Thomsen et al. 2013; Vampola 1994; Wilkinson 1994; Wu et al. 2000).

Most previous studies associated with satellite anomalies focused on the satellites in GEO. In fact, under high geomagnetic activity, more high-energy particles can be injected from the magnetotail and then precipitate into the ionosphere (Lyons 1997), possibly causing satellite anomalies in Low Earth Orbit (LEO). Ahmad et al. (2018) examined twenty anomalies recorded by the satellites in LEO and reported that these anomalies have a high positive correlation with higher geomagnetic activity. Lee et al. (2014) analyzed a significant number of anomalies recorded by two satellite missions in LEO, FORMOSAT-2 (FS2), and FORMOSAT-3/COSMIC (FS3). Their results demonstrated that the FS2 anomalies predominantly occurred in the polar region, and most of the FS3 anomalies were distributed in the South Atlantic Anomaly (SAA) region. However, that study did not include an analysis of dependences on space weather conditions, such as solar activity, geomagnetic activity, solar wind variations, etc.

The FS3 mission consists of six LEO microsatellites, and each of them has an identical structure. The FS3 satellites were launched on 15 April 2006, and their orbital altitudes and inclinations are 700–800 km and 72°, respectively. The major goal of the FS3 mission is to utilize an occultation technique for deriving the pressure and humidity of the atmosphere and the electron density of the ionosphere (Fong et al. 2009; Rocken et al. 2000). Since the FS3 mission is combined with multiple GPS satellites to establish a global atmospheric and ionospheric observing system, the FS3 mission is also called Constellation Observing System for Meteorology, Ionosphere and Climate (COSMIC). The present study endeavored to explore the characteristics of space parameters for the anomalies recorded by FS3, and particularly examined whether these anomalies were related to high geomagnetic activity. The results derived from this study can help clarify the main causes in the aspect of space weather for the FS3 anomalies.

FORMOSAT-3 anomalies

Many causes can give rise to a computer of the FS3 microsatellites resetting automatically, including ground-controlled errors, noisy transmission process, mechanical or circuit issues, software interrupts, insufficient power, larger yaw angle, abnormal attitude, etc. These common causes are divided into five categories: human-made, transmission, mechanical, circuit, and software factors. However, in addition to the factors mentioned above, the variations in space weather can cause a satellite computer to operate abnormally and auto-reset subsequently. To further understand the causes of the FS3 anomalies, computer auto-reset anomalies were classified into either space weather and non-space weather categories before analyzing them. When an auto-reset anomaly occurred in an FS3 microsatellite, the NSPO (National SPace Organization, Taiwan) staff would determine the possible cause for this anomaly and record it. If this anomaly is not made by any of the five common categories of anomaly factors, it will be classified into the category of anomalies caused by space weather effects.

Owing to the same structures and orbital parameters of all the six FS3 microsatellites, this study analyzed anomalies of these six microsatellites without differentiation. After non-space weather anomalies were removed, 626 anomalies were left for further analysis on aspects of space weather. These 626 anomalies occurred during the period from 5 May 2006 to 29 June 2016. This period is longer than that of the FS3 anomalies reported in Lee et al. (2014). Figure 1 displays the global distribution of our FS3 anomalies. It is shown that many anomalies occurred in the SAA region, as bounded in the red trapezoid. This distribution is consistent with that of the FS3 anomalies reported by Lee et al. (2014).

Methodology and results

In the subsections below, we exhibit the results of statistical examinations for the FS3 anomalies in association with different global space parameters. These results lead out our discussion that derives new understandings and relative importance of the relationships between the FS3 anomalies and these space weather parameters in the section "Discussion".

Solar wind conditions

We examined the dependences of the FS3 anomalies on solar wind conditions. To derive the relationship between the FS3 anomalies and each of the solar wind speed,

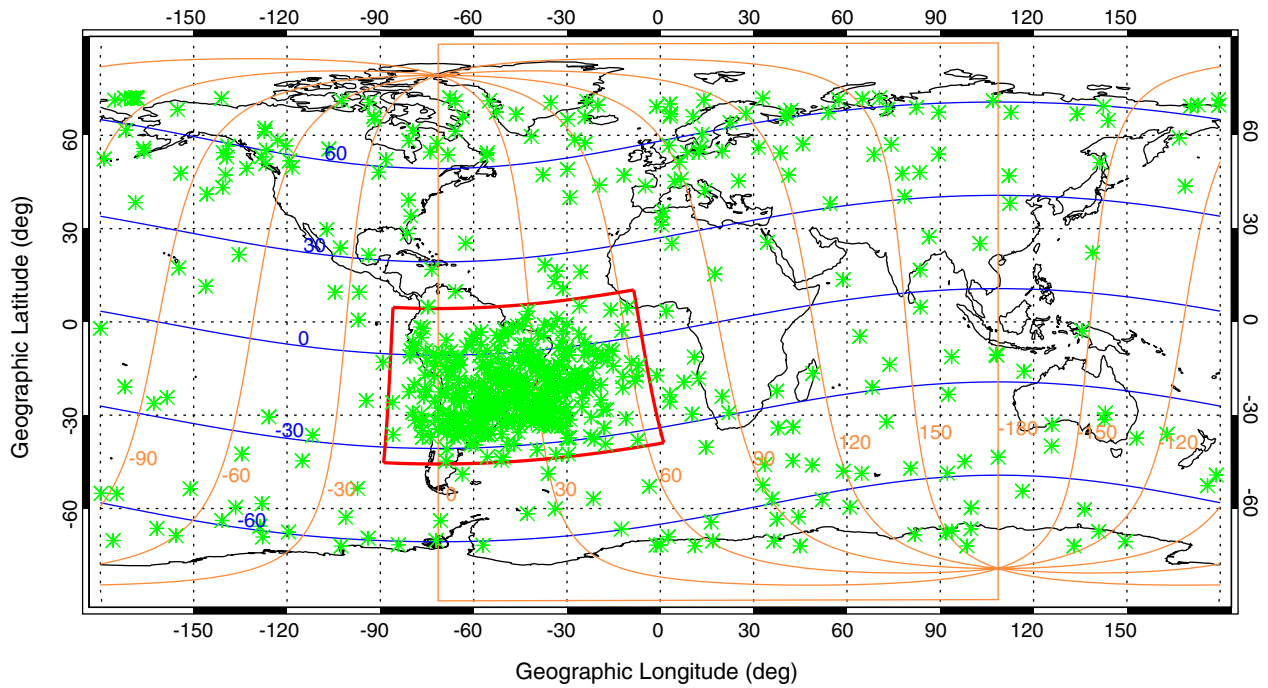

Fig. 1 Global distribution of the FS3 anomalies. The vertical and horizontal black dash lines represent various geographic longitudes and latitudes, respectively. The blue curves represent the magnetic latitudes, and the orange curves represent the magnetic longitudes. The red trapezoid marks the SAA region. The green asterisks mark the locations where the FS3 anomalies occurred

dynamic pressure, and the z component of the IMF, superposed epoch analysis was applied to these three solar wind parameters, as shown in Fig. 2. However, no significant variations in these three parameters are found before, after, or at the times of the anomalies. This indicates that high solar wind driving is not a primary cause or prerequisite of the space weather condition inducing the FS3 anomalies.

Relationship to geomagnetic activity

Many previous studies suggested that satellite anomalies are typically associated with high geomagnetic activity. To verify whether the FS3 anomalies are consistent with this finding, the Kp index (https://www.gfz-potsdam.de/en/kp-index/) was used to evaluate the state of geomagnetic activity (Allen 1982; Mayaud 1980). Since the flux of charged particles can accumulate during periods of high Kp values and persists in space environment even after the Kp value decreases, the possible influence of high geomagnetic activity by delay time was considered in this study. The daily maximum Kp value was chosen to indicate geomagnetic state, and the number of the FS3 anomalies that occurred under the condition of each Kp value was counted, as displayed in Fig. 3a. It is found that most anomalies occurred with Kp less than 4, which is generally considered as low geomagnetic activity. This result demonstrates that most of the FS3 anomalies occurred under low geomagnetic activity, but does not in itself indicate that FS3 was more likely to experience an anomaly when geomagnetic activity was low.

It is possible that the days during the mission period have more counts under low geomagnetic activity than under high geomagnetic activity. For this reason, the number of the anomalies needs to be normalized by the relative amount of time for each Kp value to determine the occurrence rate of the FS3 anomalies. Since our method used the maximum daily Kp value, this was also used for the normalization. Figure 3b shows that the occurrence rate decreases with increasing Kp value for low Kp values and then increases at a turning point near $Kp = 6$. The occurrence rate and the Kp value were therefore fitted after splitting into two intervals of $Kp \geq 6$ and $Kp \leq 6$. A linear fitting by the least-squares method for these two intervals was performed. The relationship illustrates a positive correlation for $Kp \geq 6$ and a negative correlation for $Kp \leq 6$. However, in the case that an anomaly occurred at the beginning of a particular day, the Kp value for this case was probably chosen from a 3-h interval after the anomaly. The chosen value could be highly variable, so the accuracy of the statistics will be affected. To improve the accuracy, we used a 2-day window to recalculate the anomaly occurrence rates. The

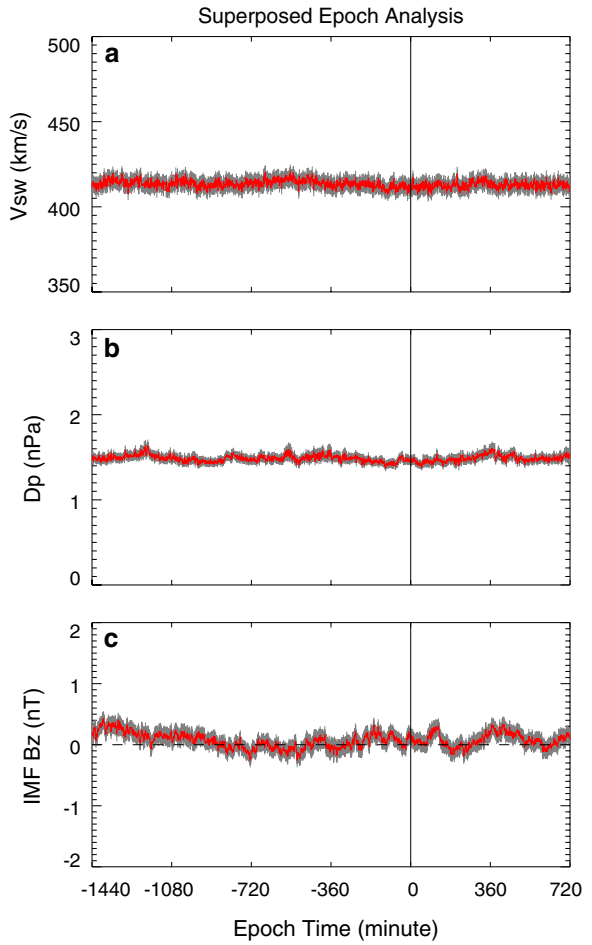

Fig. 2 Variations of solar wind parameters in reference to times of the FS3 anomalies. **a**–**c** Superposed epoch analyses on solar wind speed, dynamic pressure, and IMF *Bz*, respectively. The vertical line indicates zero epoch time, which was set to the times of the FS3 anomalies. The red curves display the variations in these three parameters. The gray areas above and below a red curve indicate standard errors

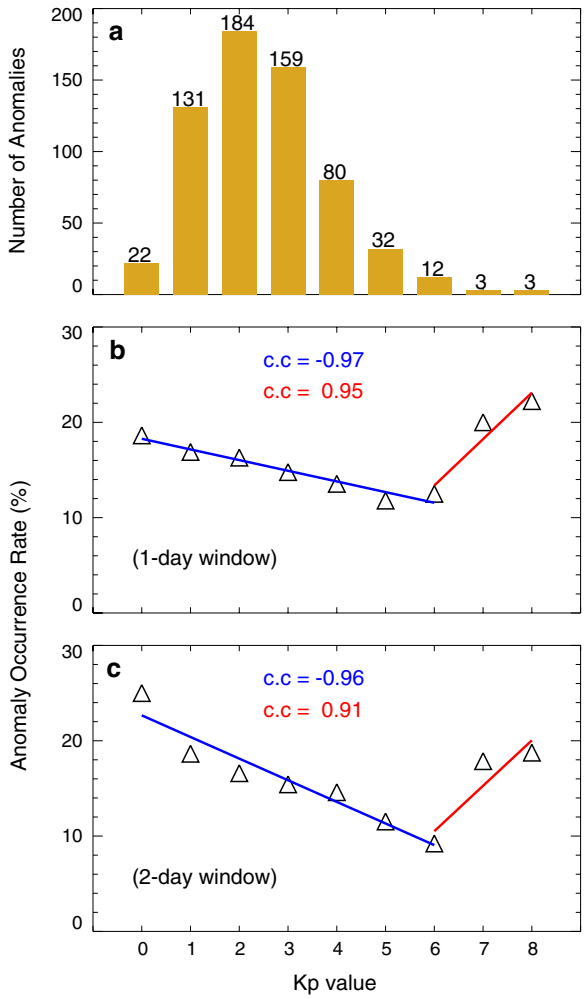

Fig. 3 Statistical analysis on the FS3 anomalies in combination with the Kp index. **a** Histogram for the numbers of FS3 anomalies in terms of the Kp values. **b**, **c** Occurrence rates of the FS3 anomalies in terms of the Kp values using the 1-day and 2-day windows for the calculation of daily Kp values, respectively. Each black triangle represents the occurrence rate in a given Kp value. The red and blue lines are the linear fittings for $Kp \geq 6$ and $Kp \leq 6$, respectively

representative Kp value for a day is the maximum Kp value in the 2 days that includes the day and the previous day. Figure 3c shows the occurrence rate of the anomalies in terms of Kp for the 2-day window. Its trend is similar to that for the 1-day window (Fig. 3b). It should be noted that the amounts of mission days with $Kp \geq 7$ are only 0.6% and 1.1% for the 1-day and 2-day windows, respectively. Therefore, if we only consider most cases of the FS3 anomalies and geomagnetic conditions ($Kp \leq 6$), the occurrence rate of the FS3 anomalies is anti-correlated with the level of geomagnetic activity.

Relationship to solar activity

As described in the section "Introduction", under high solar activity, CMEs and other special solar wind structures can frequently occur and produce more high energetic particles via shock acceleration, leading to high-speed solar wind, strong southward IMFs, and high geomagnetic activity. Most previous studies inferred these space weather conditions are more likely to spark off satellite anomalies. The number of satellite anomalies then would be expected to be higher during solar maximum than during solar minimum. However, our initial analysis did not obtain such results, in some cases obtaining the opposite results. To resolve this discrepancy, the relationship between the solar cycle and the FS3 anomalies was reexamined. The daily sunspot numbers (SSN) were averaged for individual years to determine solar

cycle variations, and then compared to the annual numbers of the FS3 anomalies. As illustrated in Fig. 4a, the number of the FS3 anomalies is the highest during solar minimum and the lowest during solar maximum. The number increases in the trailing edge of the solar cycle and decreases in the leading edge of the solar cycle. This feature illustrates an anti-correlation between the number of the FS3 anomalies and SSN.

To further investigate the relationship between the FS3 anomalies and solar activity in a shorter time scale, the occurrence rates of the FS3 anomalies in terms of SSN were calculated using the same time resolution (1 day) as the analysis of "Relationship to geomagnetic activity". The result is displayed in Fig. 4b. Considering a time delay for the influences of solar activity on Earth, here, SSN of each day is represented by the maximum value of the day and the previous day. It is found that the relationship between the occurrence rate and SSN shows a negative correlation for SSN < 120 and a positive correlation for SSN > 120. However, note that counts of SSN greater than 120 only account for a small percentage during the mission period of FS3, and most of the FS3 anomalies were accompanied with SSN lower than 120. For most cases, the occurrence rate of the FS3 anomalies is anti-correlated with the level of solar activity.

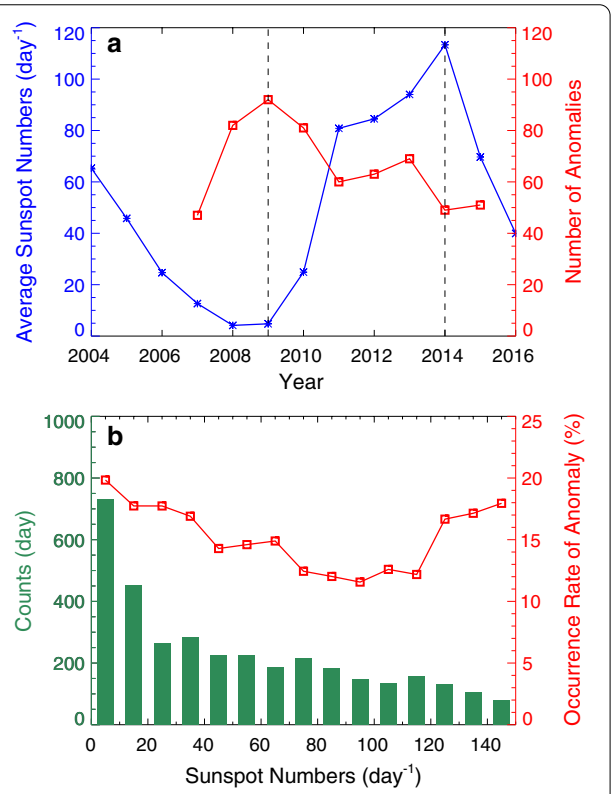

Fig. 4 Statistical analysis on the FS3 anomalies in combination with sunspot numbers. **a** Relationship between solar cycle variations and the number of the FS3 anomalies. The two dash lines denote solar minimum and solar maximum. The blue asterisks denote the yearly averages of daily sunspot numbers for individual years. The red squares indicate the numbers of the FS3 anomalies for individual years. **b** Relationship between the occurrence rate of the FS3 anomalies and sunspot numbers. The green histogram illustrates the days in terms of sunspot numbers during the mission period of FS3. The red squares represent the occurrence rates of the FS3 anomalies in terms of sunspot numbers

Relationship to galactic cosmic rays

The results presented in the previous section indicate that an FS3 anomaly did not favorably occur under high solar or geomagnetic activity, except for a small number of extreme conditions. When solar activity is high, the Sun releases more magnetic clouds into the interplanetary space. These magnetic clouds would accumulate at the heliopause and the termination shock of the solar wind, effectively blocking interstellar matter and Galactic Cosmic Rays (GCR) from entering the solar system. Therefore, the intensity of GCR observed is opposite to the level of solar activity (Zhang 2003; Schwadron et al. 2014). Moreover, Likar et al. (2012) reported that GCR can also create an anomaly on a satellite. According to the relationship between the solar cycle and the FS3 anomalies derived from the present study, it may be speculated that the GCR intensity was relatively high near the times when the FS3 anomalies occurred.

To examine the intensity of GCR at the times of the FS3 anomalies, the data of eight neutron monitors were used to conduct a superposed epoch analysis. Although the magnitudes of GCR measured at different latitudes have a larger difference during high Kp than during low Kp (Okpala 2015), they show a similar trend over time. As shown in Fig. 5a, the neutron counts detected by different monitors are in different scale ranges, and thus, we adopted their relative variations instead of their actual values for subsequent analysis. The relative variations of neutron count for each monitor can be calculated by $(C - <C>)/<C>$, where C represents neutron count and $<>$ means the average for whole interval. However, some of these monitors have data gaps at different times, and these gaps needed to be filled before we calculate relative variations of neutron count.

Figure 5b exhibits a schematic diagram for explaining how data gaps were filled. In this diagram, there are four neutron monitors for the demonstration, i.e., monitors 1–4. A data gap of monitor 1 is centered at T_A. To fill this gap, four parameters are used: T_B, A, B, and C. T_B represents the times that all monitors have values. A is the average of the values detected at T_B by monitor 1; and B (C) is the average of the values detected at T_B (T_A) by the monitors (i.e., monitors 2–4) that have values at T_A. The missing value at T_A for monitor 1 is then

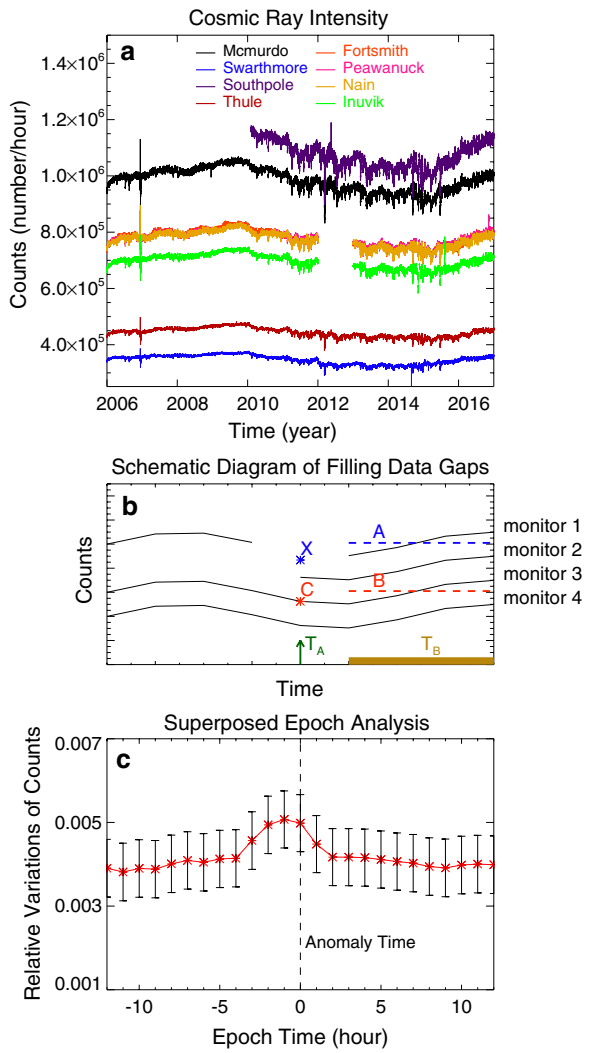

Fig. 5 Variations of the GCR intensity in reference to times of the FS3 anomalies. **a** Variations in the GCR intensity over years for different neutron monitors. Each curve in a different color represents the neutron counts detected by a neutron monitor. **b** Schematic diagram for the approach of filling data gaps of neutron monitors. The four black curves represent the variations in the neutron counts detected by four monitors. The meaning of *A*, *B*, T_A, and T_B has been elaborated in the main text. *X* is the filled value for the data gap of monitor 1 at T_A, which is calculated by $C \times A/B$. **c** A superposed epoch analysis on the relative variations of neutron count. Zero epoch time was set to the times of the FS3 anomalies. The mean value at each epoch time is marked with an asterisk. The black vertical lines indicate standard errors

calculated by $C \times A/B$. This approach was applied to the data of eight monitors used in this study. After data gaps of a monitor were filled, the relative variations of neutron count detected by this monitor can then be calculated. We averaged the relative variations of all the eight monitors at each time to produce an average curve, which was used as the relative variations of the GCR intensity.

A superposed epoch analysis on the relative variations of the GCR intensity in reference to the times of the FS3 anomalies is displayed in Fig. 5c. A peak is found during the period between 3 h before and 1 h after zero epoch time, indicating that the GCR intensity was relatively high at the times of the FS3 anomalies. This result demonstrates that one of the main causes for these anomalies was likely due to GCR.

Discussion

The present study examined the FS3 anomalies in combination with several space parameters. We find that the occurrence rate of these anomalies is anti-correlated with the level of solar or geomagnetic activity, except for extremely high conditions. Previous studies reported that high geomagnetic activity or solar activity indeed can cause satellite anomalies. Therefore, it is not surprising for those FS3 anomalies which occurred under high solar or geomagnetic activity. The intuitive effects of high solar activity and geomagnetic activity on FS3 are possibly true, but they are only for very extreme conditions and not the predominant causes of the FS3 anomalies. While it stands to reason that a satellite is more likely to experience an anomaly during high solar activity than during low solar activity, GCR could be a main source for creating a satellite anomaly during low solar activity, as shown in Figs. 4 and 5.

The anomalies used to derive the results described in the section "Methodology and results" were not specifically classified according to the anomalies within or outside the SAA region. Since Fig. 1 exhibits a higher probability of the FS3 anomalies that occurred in the SAA region, a separate analysis on the SAA and non-SAA anomalies was also conducted (not shown). The individual results for these two categories of anomalies were the same as those for all of the FS3 anomalies denoted in Fig. 1, inferring that GCR is a main source for the anomalies both within and outside the SAA region. However, one should be noted that the anomalies in the SAA region were also possibly caused by high-energy trapped protons of the inner radiation belt.

Since the magnetic fields in the inner magnetosphere do not present a perfectly symmetrical dipole, the inner radiation belt gets closer to Earth over the SAA region. Most of the FS3 anomalies occurring in this region should be related to the variations in the particle environment of the inner radiation belt. The Cosmic Ray Albedo Neutron Decay (CRAND) process is deemed to be a main source of the high-energy protons in the inner radiation belt (Albert et al. 1998; Singer 1958). During solar minimum, more GCR interacts with the atmospheric nuclei,

which increases the CRAND process and then leads to the enhancement of proton flux in the inner radiation belt. Moreover, Earth's upper atmosphere can expand to higher altitudes when it is heated by the solar extreme ultraviolet radiation. A higher neutral atmospheric density in the SAA region would cause a higher frequency of Coulomb collision between trapped protons and atmospheric particles, so the flux of high-energy protons in this region is lower during high solar activity than during low solar activity (Farley and Walt 1971; Miyoshi et al. 2000; Qin et al. 2014). Zou et al. (2015) found that the flux of high-energy trapped protons in the SAA region reduces during geomagnetic storms, and attributed the reduction to the enhancement of neutral atmospheric density (Sutton et al. 2005). As a result, the flux of high-energy trapped protons in the SAA region is anti-correlated with the trend of the solar cycle and levels of solar activity and geomagnetic activity, which is consistent with the relationship found in the FS3 anomalies that occurred mostly in the SAA region.

To our knowledge, compared with other satellites such as FS2, FS3 adopted relatively poor space specifications in the selection of the EEE (electrical, electronic, and electromechanical) parts, and the technology of radiation hardening used in FS3 was less likely to shield high energetic radiation such as GCR or high-energy trapped protons of the inner radiation belt (Fong et al. 2009; Lee et al. 2014). Additionally, FS2 was shielded well with Aluminum, whereas FS3 was not. The difference in the shielding, structure, and satellite design among FS3 and other satellites could create a difference in the dependences of anomaly occurrence rate on space weather conditions, which is worthy of a further investigation in the future.

Summary

This paper presents a statistical analysis on the dependences of the FS3 anomalies on sunspot numbers, solar wind parameters, geomagnetic activity, and the GCR intensity. It is found that most of the FS3 anomalies occurred under low geomagnetic activity, and that the occurrence rate of these anomalies is anti-correlated with the level of geomagnetic activity with an exception of a small number of extremely high geomagnetic activity ($Kp \geq 7$). Also, the number of the FS3 anomalies per year is found to be anti-correlated with the sunspot activity of the solar cycle. The results stated above are opposite to our current perception that most satellites experience more anomalies under the conditions associated with high solar activity. Furthermore, a superposed epoch analysis on the GCR intensity shows a peak value at the times when the FS3 anomalies occurred. This infers that GCR is a possible main cause for these anomalies possibly both directly and through causing increases in the flux of high-energy protons in the inner radiation belt. In summary, this paper presents a statistical result that a satellite can possibly have a high anomaly occurrence probability under low solar or geomagnetic activity.

Abbreviations

FS2: FORMOSAT-2; FS3: FORMOSAT-3; IMF: Interplanetary magnetic fields; CME: Coronal mass ejections; GEO: Geostationary earth orbit; LEO: Low earth orbit; SAA: South Atlantic anomaly; GCR: Galactic cosmic rays; SSN: Sunspot numbers; CRAND: Cosmic ray albedo neutron decay.

Acknowledgements

The authors gratefully acknowledge National Space Organization for using the list of the FS3 satellite anomalies to analyze. In addition, we would thank to GFZ German Research Centre for Geosciences for the use of the Kp data in this study.

Authors' contributions

HS and JS analyzed the data, interpreted the results, and drafted the manuscript. JD provided professional suggestions of space physics to improve the quality of this paper and help review and edit the manuscript. TL classified the FORMOSAT-3 anomalies into the categories related to space weather and non-space weather effects, and also provided the expertise on satellite structure. All authors read and approved the final manuscript.

Funding

This work was supported by the grant MOST 109-2111-M-008-007 to National Central University.

Availability of data and materials

The OMNI solar wind data were retrieved from Coordinated Data Analysis Web (https://cdaweb.sci.gsfc.nasa.gov). Since the anomaly list is a confidential document of National SPace Organization (NSPO), we are not subject to release it to the public under an agreement with NSPO. Those interested in obtaining it can directly contact Tsung-Ping Lee (kevinkohila@nspo.narl.org.tw) to apply. The data of neutron counts detected at the Mcmurdo, Swarthmore, Southpole, Thule, Fortmith, Peawanuck, Nain, and Inuvik ground stations were obtained through http://cr0.izmiran.ru/common/links.htm. The data of the *Kp* index were downloaded from https://www.gfz-potsdam.de/en/kp-index/.

Declarations

Ethics approval and consent to participate

Not applicable.

Consent for publication

Not applicable.

Competing interests

The authors have no competing interests to declare.

Author details

[1]Department of Space Science and Engineering, National Central University, Taoyuan, Taiwan. [2]School of Physics and Astronomy, University of Minnesota, Minneapolis, MN, USA. [3]National Space Organization, Hsinchu, Taiwan.

Received: 14 March 2021 Accepted: 3 May 2021
Published online: 20 May 2021

References

Ahmad N, Herdiwijaya D, Djamaluddin T, Usui H, Miyake Y (2018) Diagnosing low earth orbit satellite anomalies using NOAA-15 electron data associated with geomagnetic perturbations. Earth Planets Space 70:91. https://doi.org/10.1186/s40623-018-0852-2

Albert JM, Ginet GP, Gussenhoven MS (1998) CRRES observations of radiation belt protons 1. Data overview and steady state radial diffusion. J Geophys Res 103:9261–9273. https://doi.org/10.1029/97JA02869

Allen JH (1982) Some commonly used magnetic activity indices: Their derivation, meaning and use. In: Proceedings of a workshop on satellite drag, edited by environment research laboratories, NOAA, Boulder, Colorado, pp 114.

Anderson PC, Hanson WB, Hoegy WR (1994) Spacecraft potential effects on the Dynamics Explorer 2 satellite. J Geophys Res 99:3985–3997. https://doi.org/10.1029/93JA02104

Baker DN (2000) The occurrence of operational anomalies in spacecraft and their relationship to space weather. IEEE Trans Plasma Sci 28:2007–2016. https://doi.org/10.1109/27.902228

Bashkirov VF, Kuznetsov NV, Nymmik RA (1999) An analysis of the SEU rate of microcircuits exposed by the various components of space radiation. Radiat Meas 30:427–433. https://doi.org/10.1016/S13504487(99)00069-4

Belov A, Dorman L, Iucci N, Kryakunova O, Ptitsyna N (2004) The relation of high- and low-orbit satellite anomalies to different geophysical parameters. In: Daglis IA (editors) Effects of space weather on technology infrastructure. NATO science series II: mathematics, physics and chemistry, vol 176. Springer, Dordrecht. https://doi.org/10.1007/1-4020-2754-0_8

Choi HS, Lee J, Cho KS, Kwak YS, Cho IH, Park YD, Kim YH, Baker DN, Reeves GD, Lee DK (2011) Analysis of GEO spacecraft anomalies: space weather relationship. Space Weather 9(6):1–12. https://doi.org/10.1029/2010SW000597

Farley TA, Walt M (1971) Source and loss processes of protons of the inner radiation belt. J Geophys Res 76(34):8223–8240. https://doi.org/10.1029/JA076i034p08223

Farthing WH, Brown JP, Bryant WC (1982) Differential spacecraft charging on the geostationary operational environmental satellites. NASA technical memorandum 83908. https://ntrs.nasa.gov/archive/nasa/casi.ntrs.nasa.gov/19820018480.pdf. Accessed 7 Nov 2017

Fennell JF, Koons HC, Roeder L, Blake JB (2001) Spacecraft charging: observations and relationship to satellite anomalies. In: Harris RA (editors) Proceeding of the seventh international conference, ESTEC, Noordwijk, The Netherlands, 23–27 April 2001

Ferguson DC, Denig W, Rodriguez JV (2011) Plasma conditions during the Galaxy 15 anomaly and the possibility of ESD from subsurface charging. In: Paper presented at 49th AIAA aerospace sciences meeting including the New Horizons Forum and Aerospace Exposition, AIAA–2011-1061, Orlando, Fla., 15 Sept.

Fong CJ, Yen NL, Chu CH, Yang SK, Shiau WT, Huang CY, Chi S, Chen SS, Liou YA, Kuo YH (2009) FORMOSAT-3/COSMIC spacecraft constellation system, mission results, and prospect for follow-on mission. Terr Atmos Ocean Sci 20:1–19. https://doi.org/10.3319/TAO.2008.01.03.01(F3C)

Gonzalez WD, Joselyn JA, Kamide Y, Kroehl HW, Rostoker G, Tsurutani BT, Vasyliunas VM (1994) What is a geomagnetic storm? J Geophys Res 99(A4):5771–5792. https://doi.org/10.1029/93JA02867

Gubby R, Evans J (2002) Space environment effects and satellite design. J Atmos Terr Phys 64:1723–1733. https://doi.org/10.1016/S1364-6826(02)00122-0

Guenzer CS, Wolicki EA, Allas RG (1979) Single event upset of dynamic RAMs by neutrons and protons. IEEE Trans Nucl Sci 26:5048–5052. https://doi.org/10.1109/TNS.1979.4330270

Iucci N, Levitin AE, Belov AV, Eroshenko EA, Ptitsyna NG, Villoresi G, Chizhenkov GV, Dorman LI, Gromova LI, Parisi M, Tyasto MI, Yanke VG (2005) Space weather conditions and spacecraft anomalies in different orbits. Space Weather 3:S01001. https://doi.org/10.1029/2003SW000056

Kamide Y (1992) Is substorm occurrences a necessary condition for a magnetic storm? J Geomag Geoelec 44(2):109–117. https://doi.org/10.5636/jgg.44.109

Kolasinski WA, Blake JB, Anthony JK, Price WE, Smith EC (1979) Simulation of cosmic-ray induced soft errors and latch up in integrated-circuit computer memories. IEEE Trans Nucl Sci 26:5087–5091. https://doi.org/10.1109/TNS.1979.4330278

Lee TP, Rajesh PK, Chen CY, Liu JY, Fong CJ, Pon JC, Yang SK, Chang GS (2014) Abnormal signatures recorded by FORMOSAT-2 and FORMOSAT-3 over South Atlantic Anomaly and Polar Region. Terr Atmos Ocean Sci 25:573–580. https://doi.org/10.3319/TAO.2014.02.26.01(AA)

Likar JJ, Bogorad AL, Lombardi RE, Stone SE, Herschitz R (2012) On-Orbit SEU rates of UC1864 PWM: comparison of ground based rate calculations and observed performance. IEEE Trans Nucl Sci 59:3148–3153. https://doi.org/10.1109/TNS.2012.2224128

Liu Y, Luhmann JG, Bale SD, Lin RP (2011) Solar source and heliospheric consequences of the 2010 April 3 coronal mass ejection: a comprehensive view. Astrophys J 734(2):84. https://doi.org/10.1088/0004-637X/734/2/84

Lohmeyer W, Carlton A, Wong F, Bodeau M, Kennedy A, Cahoy K (2015) Response of geostationary communications satellite solid-state power amplifiers to high-energy electron influence. Space Weather 13:298–315. https://doi.org/10.1002/2014SW001147

Lotoaniu TM, Singer HJ, Rodriguez JV, Green J, Denig W, Biesecker D, Angelopoulos V (2015) Space weather conditions during the Galaxy 15 spacecraft anomaly. Space Weather 13:484–502. https://doi.org/10.1002/2015SW001239

Love DL, Toomb DS, Wilkinson DC, Parkinson JB (2000) Penetrating electron fluctuations associated with GEO spacecraft anomalies. IEEE Trans Plasma Sci 28:2075–2084. https://doi.org/10.1109/27.902234

Lyons LR (1997) Magnetospheric processes leading to precipitation. Space Sci Rev 80:109–132. https://doi.org/10.1023/A:1004977704864

Mayaud PN (1980) Derivation, meaning and use of geomagnetic indices, geophysical monograph series, vol 22. American Geophysical Union, Washington. https://doi.org/10.1029/GM022

Miyoshi Y, Morioka A, Misawa H (2000) Long term modulation of low altitude proton radiation belt by the Earth's atmosphere. Geophys Res Lett 27(14):2169–2172. https://doi.org/10.1029/1999GL003721

Möstl C, Temmer M, Rollett T, Farrugia CJ, Liu Y, Veronig AM, Leitner M, Galvin AB, Biernat HK (2010) STEREO and Wind observations of a fast ICME flank triggering a prolonged geomagnetic storm on 5–7 April 2010. Geophys Res Lett 37:0094–8276. https://doi.org/10.1029/2010GL045175

Nichitiu F, Drummond JR, Zou J, Deschambault R (2004) Solar particle events seen by the MOPITT instrument. J Atmos Terr Phys 66:1797–1803. https://doi.org/10.1016/j.jastp.2004.06.002

O'Brien TP (2009) SEAS-GEO: a spacecraft environmental anomalies expert system for geosynchronous orbit. Space Weather 7(9):1. https://doi.org/10.1029/2009SW000473

Okpala KC (2015) Galactic cosmic ray variability at two neutron monitors: relation to Kp index. J Astrophys 2015:1–5. https://doi.org/10.1155/2015/961358

Pilipenko V, Yagova N, Romanova N, Allen J (2006) Statistical relationship between satellite anomalies at geostationary orbit and high-energy particles. Adv Space Res 37(6):1192–1205. https://doi.org/10.1016/j.asr.2005.03.152

Qin M, Zhang X, Ni B, Song H, Zou H, Sun Y (2014) Solar cycle variations of trapped proton flux in the inner radiation belt. J Geophys Res Space Phys 119:9658–9669. https://doi.org/10.1002/2014JA020300

Rocken C, Kuo Y, Schreiner W, Hunt D, Sokolovskiy S, Mccormick C (2000) COSMIC system description. Terr Atmos Ocean Sci 11(1):021–052. https://doi.org/10.3319/TAO.2000.11.1.21(COSMIC)

Schwadron NA, Blake JB, Case AW, Joyce CJ, Kasper J, Mazur J, Petro N, Quinn M, Porter JA, Smith CW, Smith S, Spence HE, Townsend LW, Turner R, Wilson JK, Zeitlin C (2014) Does the worsening galactic cosmic radiation environment observed by CRaTER preclude future manned deep space exploration? Space Weather 12:622–632. https://doi.org/10.1002/2014SW001084

Singer SF (1958) Trapped albedo theory of the radiation belt. Phys Rev Lett 1:181–183. https://doi.org/10.1103/PhysRevLett.1.181

Sutton EK, Forbes JM, Nerem RS (2005) Global thermospheric neutral density and wind response to the severe 2003 geomagnetic storms from CHAMP accelerometer data. J Geophys Res. https://doi.org/10.1029/2004JA010985

Thomsen MF, Henderson MG, Jordanova VK (2013) Statistical properties of the surface-charging environment at geosynchronous orbit. Space Weather 11(5):237–244. https://doi.org/10.1002/swe.20049

Vampola AL (1994) Analysis of environmentally induced spacecraft anomalies. J Spacecraft Rockets 31(2):154–159. https://doi.org/10.2514/3.26416

Wilkinson DC (1994) National Oceanic and Atmospheric Administration's spacecraft anomaly data base and examples of solar activity affecting spacecraft. J Spacecr Rockets 31:160–165. https://doi.org/10.2514/3.26417

Wu JG, Eliasson L, Lundstedt H, Hilgers A, Andersson L, Norberg O (2000) Space environment effects on geostationary spacecraft: analysis and

prediction. Adv Space Res 26(1):31–36. https://doi.org/10.1016/S0273-1177(99)01023-6
Zhang M (2003) Modulation of galactic cosmic rays at solar maximum: observations. Adv Space Res 32:603–614. https://doi.org/10.1016/S0273-1177(03)00347-8
Zou H, Li C, Zong Q, Parks GK, Pu Z, Chen H, Xie L, Zhang X (2015) Short-term variations of the inner radiation belt in the South Atlantic Anomaly. J Geophys Res Space Phys. https://doi.org/10.1002/2015JA021312

Publisher's Note